Ultrasound in Med. & Biol., Vol. 43, No. 11, pp. 2537–2545, 2017

0301-5629/$ - see front matter

http://dx.doi.org/10.1016/j.ultrasmedbio.2017.06.016

● *Original Contribution*

ULTRASOUND IMAGING OF MUSCLE CONTRACTION OF THE TIBIALIS ANTERIOR IN PATIENTS WITH FACIOSCAPULOHUMERAL DYSTROPHY

Kaj Gijsbertse,* Rianne Goselink,† Saskia Lassche,† Maartje Nillesen,‡ André Sprengers,*§ Nico Verdonschot,*§ Nens van Alfen,† and Chris de Korte‡¶

*Orthopaedic Research Laboratory, Department of Orthopaedics, Radboud university medical center, Nijmegen, The Netherlands; †Department of Neurology, Donders Centre for Neuroscience, Radboud university medical center, Nijmegen, The Netherlands; ‡Medical Ultrasound Imaging Center (MUSIC), Department of Radiology and Nuclear Medicine, Radboud university medical center, Nijmegen, The Netherlands; §Laboratory of Biomechanical Engineering, University of Twente, Enschede, The Netherlands; and ¶Physics of Fluids Group, MESA+ Institute for Nanotechnology and MIRA Institute for Biomedical Technology and Technical Medicine, University of Twente, Enschede, The Netherlands

(*Received* 24 *March* 2017; *revised* 14 *June* 2017; *in final form* 16 *June* 2017)

Abstract—A need exists for biomarkers to diagnose, quantify and longitudinally follow facioscapulohumeral muscular dystrophy (FSHD) and many other neuromuscular disorders. Furthermore, the pathophysiological mechanisms leading to muscle weakness in most neuromuscular disorders are not completely understood. Dynamic ultrasound imaging (B-mode image sequences) in combination with speckle tracking is an easy, applicable and patient-friendly imaging tool to visualize and quantify muscle deformation. This dynamic information provides insight in the pathophysiological mechanisms and may help to distinguish the various stages of diseased muscle in FSHD. In this proof-of-principle study, we applied a speckle tracking technique to 2-D ultrasound image sequences to quantify the deformation of the tibialis anterior muscle in patients with FSHD and in healthy controls. The resulting deformation patterns were compared with muscle ultrasound echo intensity analysis (a measure of fat infiltration and dystrophy) and clinical outcome measures. Of the four FSHD patients, two patients had severe peroneal weakness and two patients had mild peroneal weakness on clinical examination. We found a markedly varied muscle deformation pattern between these groups: patients with severe peroneal weakness showed a different motion pattern of the tibialis anterior, with overall less displacement of the central tendon region, while healthy patients showed a non-uniform displacement pattern, with the central aponeurosis showing the largest displacement. Hence, dynamic muscle ultrasound of the tibialis anterior muscle in patients with FSHD revealed a distinctively different tissue deformation pattern among persons with and without tibialis anterior weakness. These findings could clarify the understanding of the pathophysiology of muscle weakness in FSHD patients. In addition, the change in muscle deformation shows good correlation with clinical measures and quantitative muscle ultrasound measurements. In conclusion, dynamic ultrasound in combination with speckle tracking allows the study of the effects of muscle pathology in relation to strength, force transmission and movement generation. Although further research is required, this technique can develop into a biomarker to quantify muscle disease severity. (E-mail: Kaj.Gijsbertse@radboudumc.nl)

Key Words: **Ultrasound, Facioscapulohumeral muscular dystrophy, Skeletal muscle, Speckle tracking, Deformation imaging.**

INTRODUCTION

In many neuromuscular diseases, a need exists for biomarkers to characterize the severity and pattern of muscle involvement. With advances in the quality and availability of radiologic technologies, the role of muscle imaging is growing in the evaluation of patients with suspected neuromuscular disorders (Simon et al. 2016). Skeletal muscle imaging is used as a diagnostic tool to screen and identify the presence and pattern of pathology, and can be used to guide muscle biopsies. Ultrasound (US) has well-recognized advantages of being an cost-effective, non-ionizing, point-of-care imaging modality with proven clinical validity in detecting neuromuscular disorders (Arts et al. 2012; Heckmatt et al. 1980; Pillen et al. 2008; Simon et al. 2016; Zaidman and van Alfen

Address correspondence to: Kaj Gijsbertse, Geert Grooteplein Zuid 10. P.O. Box 9101, NL-6500 HB, Nijmegen, The Netherlands. E-mail: Kaj.Gijsbertse@radboudumc.nl

2016). Previous studies have shown that static US images can be of value in the diagnosis of neuromuscular disorders by enabling the assessment of muscle thickness and the quantification of muscle atrophy (or hypertrophy) and muscle morphology changes (Janssen et al. 2014a; Pillen et al. 2007; Raiteri et al. 2016; Reimers et al. 1993; Zaidman and van Alfen 2016). Neuromuscular disorders can lead to an increase in muscle echo intensity (*i.e.,* a muscle becomes whiter in appearance). An increase in fat and fibrous tissues is responsible for the high echo intensity appearance of muscles, as they increase the number of reflections within the muscle and therefore the mean gray value (echogenicity) of the muscle in the ultrasound image (Pillen et al. 2009; Pillen and van Alfen 2011).

Facioscapulohumeral muscular dystrophy (FSHD) is one of the most common forms of hereditary myopathy in adults (Deenen et al. 2015; Lunt et al. 1995). It derives its name from the muscle groups that are mainly affected at the initial stage of the disease: facial and shoulder girdle muscles. The disease is characterized by asymmetric loss of force and atrophy of muscular tissue starting in the face and shoulder region, with early involvement of the tibialis anterior in many patients (Mul et al. 2016; Tawil 2008).

Although we can monitor the progress of neuromuscular diseases using imaging techniques, the pathophysiological mechanisms that lead to muscle weakness in various muscle disorders, such as FSHD, are not completely understood. With disease progression, healthy muscle tissue will increasingly be replaced by fat and fibrosis. This process can be quite asymmetric and variable along the length of the muscle in FSHD (Janssen et al. 2014b). Because fat and fibrosis do not have electrically activated contractile properties, these tissues will not contribute to force production during muscle contractions. However, this may not be the only reason that force production changes during disease progression. On the one hand, the progression of muscle tissue replacement not only decreases the amount of muscle tissue available for contraction, but also very likely decreases force transduction throughout the dystrophic segments to the tendons. On the other hand, even individual FSHD muscle fibers have decreased contractile properties (Lassche et al. 2013).

Quantification of tissue deformation during contraction will be of interest in fundamental and clinical questions with respect to changes in functional behavior of muscles at various stages of the dystrophic process in FSHD. Measuring local skeletal muscle deformation *in vivo* might provide new insights how pathologic muscle tissue contracts and transmits force, which leads to a better understanding of weakness in muscle disease and might provide a functional outcome measurement to study disease evolution.

Therefore, in this explorative study, we examined muscle tissue deformation during *in vivo* contractions of the tibialis anterior muscle in patients with various clinical stages of FSHD and healthy controls, by using dynamic 2-D ultrasound imaging combined with speckle tracking.

MATERIALS AND METHODS

Patients

This observational study was conducted at the Radboud University Medical Center, Nijmegen, The Netherlands. Four patients with a DNA-confirmed diagnosis of FSHD who regularly visited the outpatient clinic and four healthy controls were included. Data were obtained August 2016–December 2016. All patients gave their informed consent according to the approval from our institutional review board. The study was performed in accordance with the World Medical Association Declaration of Helsinki on Ethical Principles for Medical Research Involving Human Patients.

Clinical assessment

The following clinical measurements were collected: age, gender, height, weight and manual muscle testing scores of the tibialis anterior muscle using the Medical Research Council (MRC) grading system (Vanhoutte et al. 2012). The age-adjusted clinical severity scale (Ricci et al. 1999; van Overveld et al. 2005) and the FSHD evaluation score (Lamperti et al. 2010) were assessed. Both scales have demonstrated a good inter- and intra-reliability in adults. In addition, the *walking on heels* test of the Motor Function Measure (Berard et al. 2005) was used as a specific functional measurement for tibialis anterior muscle strength. The tibialis anterior muscle was chosen for its good accessibility to US imaging, and because studies have shown that this muscle is one of the most early and severely involved muscles in the lower extremities in FSHD (Janssen et al. 2014a,b; Mul et al. 2016; Tasca et al. 2012).

Ultrasound data acquisition

All US examinations were performed on a MyLab Twice US system (Esaote, Genoa, Italy), using a 3–13 MHz broadband linear transducer (LA533) with an axial and lateral image resolution of 0.3 mm and 0.9 mm, respectively. Patients were examined in a supine, relaxed position. US data were acquired at the muscle belly of the tibialis anterior with a standardized transducer location at one-third of the distance on the line from interior aspect of the patella to the lateral malleolus (Scholten et al. 2003). The tibialis anterior muscle was identified on the US image and a region of interest

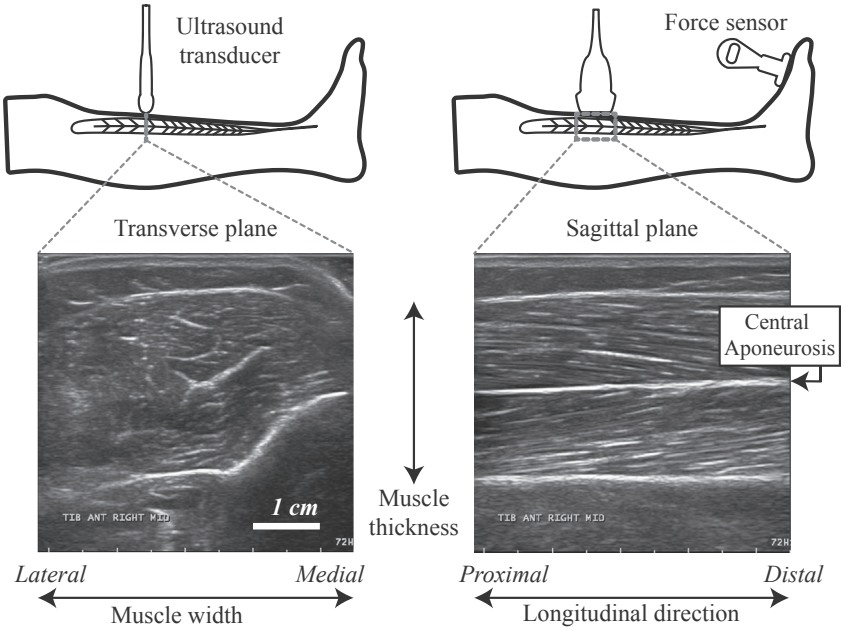

Fig. 1. Transducer positions for measuring the tibialis anterior and example US images. US imaging sequences were acquired during an isometric contraction in the sagittal plane (*right panel*). Muscle atrophy was determined using gray-scale analysis (echogenicity) of static US data in the transverse plane (*left panel*). US = ultrasound.

(ROI) was drawn manually in the US images by two different experienced clinicians (N.v.A. and S.L.). US image sequences were acquired from both legs with the US transducer placed longitudinally, creating a sagittal plane representation of the muscle (Fig. 1, *right panel*). In this plane, the (dominant) translational motion of the muscle was visualized. Patients were instructed to contract their foot dorsiflexors maximally for 3 s while their foot was constrained by a dynamometer (CITEC, CIT Technics, Haren, The Netherlands) that recorded the maximum exerted force during the contraction. During the contraction of the muscle, US data were acquired in Digital Imaging and Communications in Medicine (DICOM) format at a frame rate of 25 Hz.

Speckle tracking of dynamic muscle US

Tissue displacement was computed retrospectively using a customized MATLAB-based (MathWorks Inc., Natick, MA, USA) 2-D displacement estimation and tracking algorithm, which was developed and validated on simulated, phantom and *in vivo* data (Gijsbertse et al. 2017; Lopata, et al. 2009, 2010). This algorithm estimates the displacement between two consecutive frames by cross correlating 2-D segments of US data. A grid of nodes (spaced apart 0.5 mm in the axial and 1 mm in the lateral direction) was positioned within the ROI, at every node, displacement estimations were calculated. A kernel of US data (5.2 × 2.9 mm) centered on the nodes was cross correlated with a larger search kernel (14.6 × 5.7 mm) within the consecutive frame. For sub-pixel displacement estimation, the cross-correlation peak was detected using spline fitting of the cross-correlation function. Inter-frame axial and lateral displacement estimations were filtered with a median filter of 5 × 5 mm to remove outliers.

Accumulated displacement estimates throughout the entire contraction were computed from the inter-frame displacements using bilinear interpolation (Lopata et al. 2009). The longitudinal displacement maps of the muscles at their maximum contraction were visualized on top of the B-mode images, and muscle motion was expressed as the average longitudinal displacement within the ROI. Additionally, the longitudinal displacement maps of all patients were compared at time points where the averaged longitudinal displacement matched. This allowed us to compare the deformation pattern at the same level of muscle motion.

Table 1. Clinical data of patients and healthy controls

Subject no.	Age	Gender	MRC score [left, right]	FSHD score
HC1	24	Man	-	-
HC2	32	Man	-	-
HC3	47	Woman	-	-
HC4	27	Woman	-	-
pat1	31	Woman	[5,5]	2
pat2	24	Man	[4,4]	3
pat3	50	Man	[3,3]	8
pat4	37	Man	[2,3]	12

FSHD = facioscapulohumeral muscular dystrophy; HC# = healthy volunteer number; pat# = patient number.

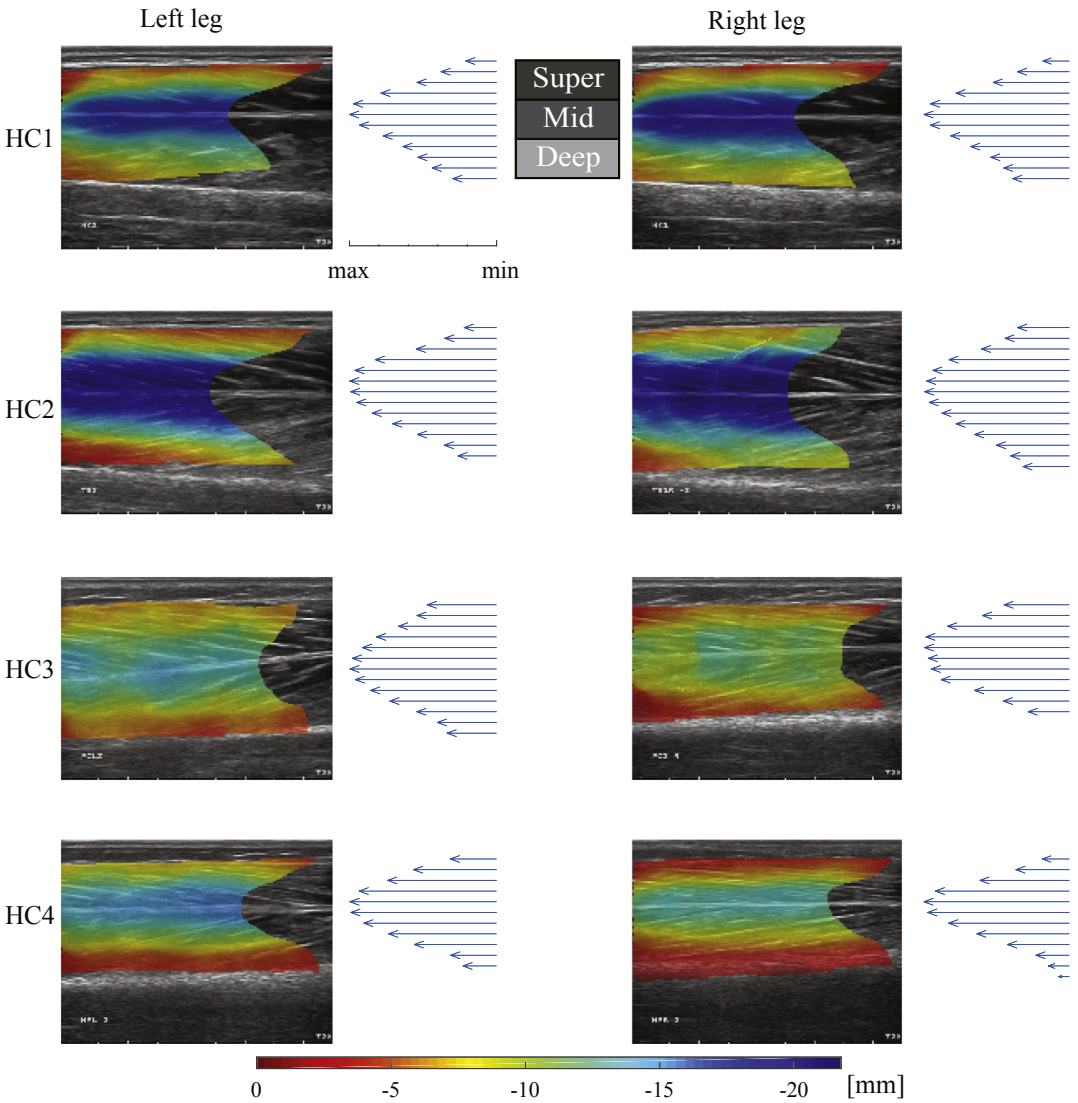

Fig. 2. Muscle tissue displacement of four healthy controls at their maximum voluntary contraction. The displacement maps depict the longitudinal displacement (mm) of the muscle in the sagittal ultrasound plane. The *arrows* represent the averaged normalized muscle displacement (displacement profile) across the thickness of the muscle; the mid region at the central aponeurosis shows the largest displacement.

Displacement profiles were computed by averaging the longitudinal displacements across the thickness of the muscle and normalized to their maximum measured displacement to allow comparison among patients. The displacement profiles were expressed as quiver plots.

Quantitative analysis of static US images

For quantitative muscle gray-scale analysis, or *echogenicity* measurement, 3 images were obtained of tibialis anterior muscles of the left and right leg in the transverse plane (Fig. 1, *left panel*), using a standardized scanning protocol with a fixed preset and image parameters, as previously described in Scholten et al. (2003). Echogenicity was determined offline by averaging the mean gray value (on a scale 0–255) of the 3 measurements from the ROI. Muscle echogenicity was then compared with tibialis anterior–specific echogenicity reference values (Nijboer-Oosterveld et al. 2011), which are corrected for gender, age, height and weight and results were expressed as a z-score (*i.e.,* the number of standard deviations from the mean) (Pillen et al. 2003). A z-score of >2 (*i.e.*, a gray value larger than the value for 95% of the population) was considered abnormal.

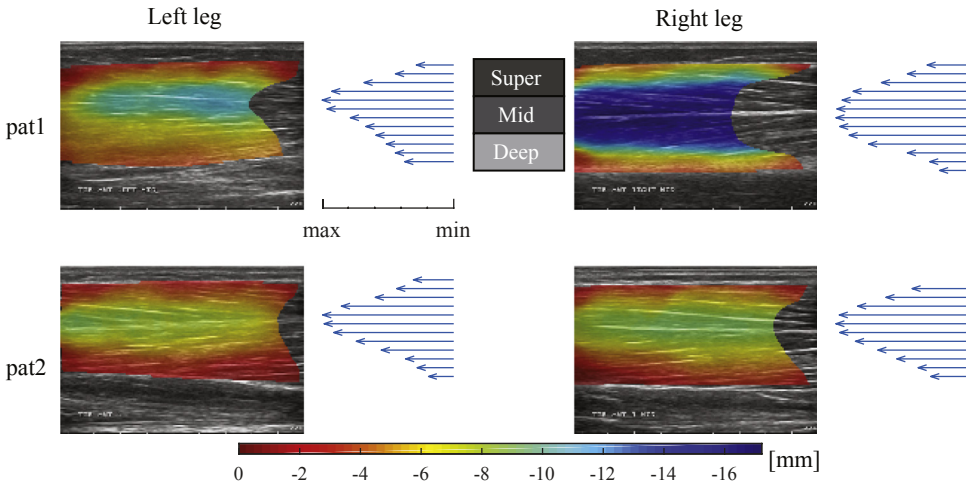

Fig. 3. Muscle tissue displacement of pat1 and pat2 with mild peroneal weakness. Although the average displacement is slightly lower than healthy controls, the displacement patterns are similar; the mid region at the central aponeurosis shows the largest motion. pat# = patient number.

RESULTS

Table 1 summarizes the clinical data of the patients and healthy controls. Four patients with genetically confirmed FSHD were included with clinical FSHD scores ranging 2–12. Two patients (3 and 4) had peroneal weakness (MRC ≤3) and two patients only had mildly peroneal weakness on clinical examination.

The longitudinal tissue displacement of the tibialis anterior of all healthy patients at maximum contraction is shown in Figure 2. For all healthy patients a non-uniform deformation pattern was observed across the thickness of the muscle, with the middle region at the central aponeurosis consistently exhibiting larger displacements than the superficial and deep outer layers of the muscle. The normalized displacement profiles show a parabolic shape with steep flanks. The average longitudinal tissue displacement within the ROI of all healthy patients was -9.7 ± 1.8 mm.

Patients with only mild tibialis anterior weakness (1 and 2) showed similar deformation patterns as healthy patients (Fig. 3), but the average tissue displacement was slightly lower than the healthy controls (-6.5 ± 2.5 mm).

Two patients (3 and 4) showed severe tibialis anterior weakness at clinical examination. Dynamic US data revealed that the muscle tissue displacement of these patients was lower (-2.1 ± 1.0 mm) and deformed in a completely different manner. In Figure 4, the displacement of muscle tissue of patient 3 is depicted. The deformation pattern is almost homogenous across the thickness of the muscle, with the superficial and deeper regions of the muscle exhibiting similar displacement as the middle region. Patient 4 was the most severely affected patient in this study. We observed a uniform deformation pattern in the superficial and mid region of the muscle at maximum contraction, while the deeper region showed almost no tissue displacement, with a tendency in the opposite direction of the contraction (Fig. 5).

All muscle deformation patterns were analyzed at the point of maximum muscle motion. Additionally, the difference in the muscle deformation patterns among

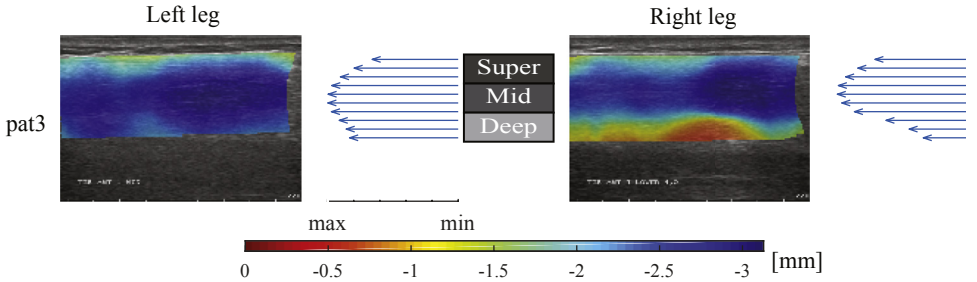

Fig. 4. Muscle tissue displacement of pat3 with severe peroneal weakness. The displacement maps are more homogenous across the thickness of the muscle. The superficial and deeper regions are exhibiting almost equal displacement as the mid region. pat# = patient number.

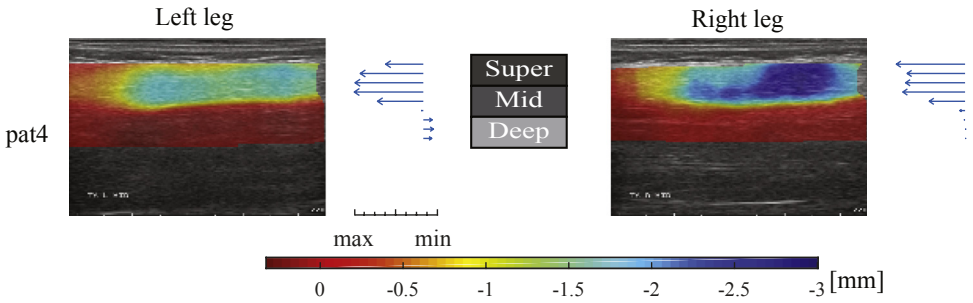

Fig. 5. Muscle tissue displacement of pat4 with severe peroneal weakness. The superficial and mid region of the muscle show a homogenous displacement pattern along the depth, but the deeper region shows almost no motion with a tendency in the opposite direction than the contraction direction. pat# = patient number.

patients without and patients with peroneal weakness was independent of the contraction phase. For equal muscle tissue displacement (for patients at their plateau and for healthy patients early in the contraction phase), the variation in deformation pattern was already visible (Fig. 6).

The resulting deformation patterns were compared with muscle echogenicity values, clinical outcome measures and maximum exerted force and showed good agreement (Table 2). Similar to the averaged measured displacement in the muscles, the peak force measurements acquired by the dynamometer showed that FSHD patients produced less muscle force than the healthy controls (56 ± 45 N vs. 162 ± 20 N). Figure 7 shows the good correlation between measured force and muscle motion,

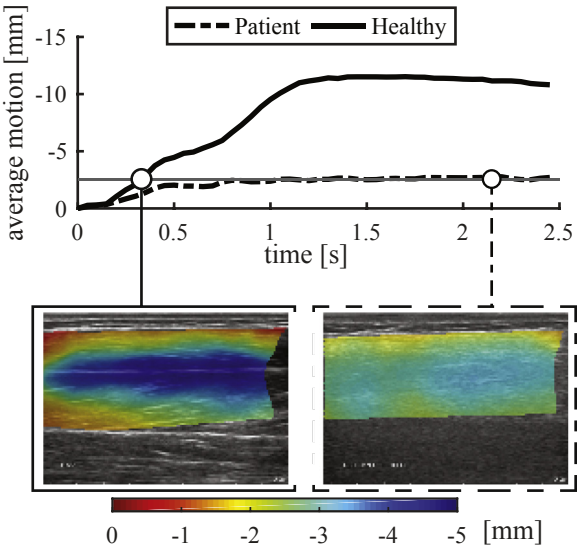

Fig. 6. Muscle displacement maps of HC#1 and a severely affected patient (pat3) with peroneal weakness. The selected frames are matched according to their average measured muscle tissue displacement. The displacement patterns within the muscles are quite varied, which indicates that for similar muscle *activity* a difference exists in functional behavior. HC# = healthy volunteer number; pat# = patient number.

with a linear coefficient of determination (R^2 value) of 0.91. In addition to the detected weakness, US echogenicity z-scores were highest for patients with clear tibialis anterior weakness with z-scores 2.7–4.78, corroborating that these muscles were (severely) affected. The echogenicity of patients with only mild tibialis anterior weakness were considered normal, because the z-scores did not exceed levels >2.

DISCUSSION

The results of this explorative study suggest that the deformation pattern of the tibialis anterior muscle with abnormal echogenicity is different from that of a healthy or only mildly affected muscle without clear US abnormalities. Severely affected muscles most notably show decreased motion of the central tendon aponeurosis of the tibialis anterior, which strongly suggests a decrease in force transferred to this central tendon and, hence, a decrease in force output when attempting to flex the ankle. In the most severely affected patient, a part of the muscle even showed a very small paradoxical movement, suggesting that this part of the muscle no longer actively participated in the contractile process, but was rather moved in a passive fashion as result of other still contractile muscle parts.

The observed difference in displacement patterns for equal muscle motion (Fig. 6) indicate that the change in deformation is not a result of lower muscle *activity*, as seen in severely affected patients, but suggests a change in functional behavior and force transmission of affected muscles. Matching the muscle activity among patients is difficult, because we did not have continuous force measurements. Electronically triggered contraction (*i.e.,* twitch contraction) would allow us to study displacement and strain rate in a more controlled fashion (Lopata et al. 2010). This would also eliminate the possibility of co-contraction effects. Stimulation, however, is not very comfortable and may introduce additional practical problems.

Table 2. US findings: Gray-scale analysis (z-score) and muscle deformation findings

Subject no.	Leg	Peroneal weakness	Force (N)	z-score	Muscle motion (mm)	Muscle tissue displacement findings
HC1	Left	No	175	−2.19	−10.5	Non-uniform deformation pattern, with the muscle region at central aponeurosis showing the largest displacement. The muscle displacement profile shows a parabolic shape.
	Right		200	−2.41	−11.1	
HC2	Left	No	165	0.83	−11.4	
	Right		164	0.05	−11.9	
HC3	Left	No	140	−0.07	−9.1	
	Right		145	0.38	−7.7	
HC4	Left	No	170	−0.36	−9.2	
	Right		140	−0.17	−6.8	
pat1	Left	Mild	102	−0.46	−6.0	Similar to healthy patients: largest displacement at central aponeurosis.
	Right		130	−0.36	−10.2	
pat2	Left	Mild	79	1.44	−4.7	Similar to healthy patients: largest displacement at central aponeurosis.
	Right		70	0.21	−5.13	
pat3	Left	Severe	33	3.60	−3.1	Homogenous/uniform displacement pattern. Parabolic profile is diminished.
	Right		14	2.70	−2.6	
pat4	Left	Severe	10	3.80	−0.9	Homogenous and uniform displacement pattern in superficial region and inverted displacement in deep region.
	Right		13	4.47	−1.6	

HC# = healthy volunteer number; pat# = patient number.

Despite that voluntary muscle contractions may not be an accurate way to determine the maximum force, the force measurements indicate that muscles of patients with normal echogenicity and deformation patterns were weaker. This suggests the existence of a qualitative mechanism of muscle weakness based on a loss of intrinsic contractile strength. Lassche et al. (2013) demonstrated a reduction in sarcomeric force in type II FSHD muscle fibers, which could play a role in the development of muscle weakness. Unpublished work by our group corroborates that atrophy and fat infiltration by themselves cannot explain the reduced muscle force, as they calculated lower specific muscle tension from musculoskeletal models, which compensated for the loss of functional muscle tissue. Furthermore, the distal to proximal progression of fat and fibrotic tissue infiltration not only decreases the amount of muscle tissue available for contraction but also very likely decreases force transduction and deformation pattern throughout the dystrophic segments to the distal tendon (Lacourpaille et al. 2014). Subsequent studies that quantify muscle contraction along the entire length of the muscle are required to reveal local differences in contraction patterns. A multidimensional imaging modality is needed for a comprehensive mapping of muscle contraction. Besides, the limited field-of-view, 2-D displacement estimation techniques are also prone to errors as a result of out-of-plane motion that can arise from muscle twist. Although we were unable to capture the out-of-plane motion, we are confident in the robustness of this method to track motion within the image plane as the peak normalized cross-correlation values were high and qualitative inspection did not reveal significant out-of-plane motion. The work presented here utilizes DICOM data, and the accuracy of the displacement estimation may benefit from the use of raw US data (RF data). This increases the axial (along the US beam) resolution. Additionally, the estimation of the lateral displacement can be improved using compounding techniques, as described by Hansen et al. 2010. However, these techniques require dedicated equipment and sequences and access to RF data, which are not typically available on US machines used in clinical practice. Three-dimensional US techniques have been applied to study the contraction of skeletal muscles (Deffieux et al. 2008; Gijsbertse et al. 2017; Raiteri et al. 2016). However, a trade-off exists among spatial resolution, field-of-view and temporal resolution in these 3-D

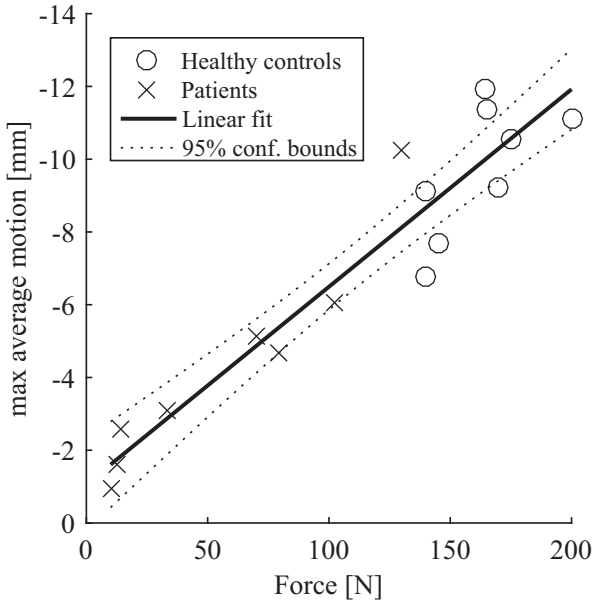

Fig. 7. Linear regression of peak force [N] and muscle motion [mm]. R^2 value = 0.91.

techniques. Alternatively, magnetic resonance imaging (MRI) allows the study of muscle contraction throughout the full length of the muscle (Dresner et al. 2001; Englund et al. 2011; Mazzoli et al. 2016; Moerman et al. 2012; Pappas et al. 2002; Zhong et al. 2008). While MRI measurements can provide detailed information about muscle structures, its ability to quantify muscle deformation during natural activities (*e.g.,* gait) is limited. US imaging systems are developing toward portable systems that allow us to study muscle contraction during highly dynamic tasks (Eranki et al. 2013).

Our findings as presented in this study are based on a small group of healthy controls and patients diagnosed with FSHD. More extensive studies are needed to confirm these data. Longitudinal studies that provide insight in the change of muscle functioning as a function of disease progression may help us understand why muscles in neuromuscular diseases become weaker. Local assessment of muscle deformation can be of interest in many other neuromuscular diseases, such as inclusion body myositis. Furthermore, speckle tracking also provides a tool to extract detailed information of the presence of fasciculations or fibrillations as seen in motor neuron diseases (Harding et al. 2016).

In conclusion, this work provides a tool to quantify muscle motion and evidence of changing functional behavior of affected muscles in FSHD patients. The quantitative characterization of muscle contraction provides new insights in the way pathologic muscle tissue deforms and transmits force, which leads to a better understanding of the underlying phenomena related to weakness in muscle disease.

Acknowledgments—The research leading to these results has received funding from the European Research Council under the European Union's Seventh Framework Programme (FP/2007-2013)/ERC Grant Agreement n. 323091 awarded to N. Verdonschot.

REFERENCES

Arts IM, Overeem S, Pillen S, Kleine BU, Boekestein WA, Zwarts MJ, Jurgen Schelhaas H. Muscle ultrasonography: A diagnostic tool for amyotrophic lateral sclerosis. Clin Neurophysiol 2012;123:1662–1667.

Berard C, Payan C, Hodgkinson I, Fermanian J. A motor function measure scale for neuromuscular diseases. Construction and validation study. Neuromuscul Disord 2005;15:463–470.

Deenen JC, Horlings CG, Verschuuren JJ, Verbeek AL, van Engelen BG. The epidemiology of neuromuscular disorders: A comprehensive overview of the literature. J Neuromuscul Dis 2015;2:73–85.

Deffieux T, Gennisson JL, Tanter M, Fink M. Assessment of the mechanical properties of the musculoskeletal system using 2-D and 3-D very high frame rate ultrasound. IEEE Trans Ultrason Ferroelectr Freq Control 2008;55:2177–2190.

Dresner MA, Rose GH, Rossman PJ, Muthupillai R, Manduca A, Ehman RL. Magnetic resonance elastography of skeletal muscle. J Magn Resonance Imaging 2001;13:269–276.

Englund EK, Elder CP, Xu Q, Ding Z, Damon BM. Combined diffusion and strain tensor MRI reveals a heterogeneous, planar pattern of strain development during isometric muscle contraction. Am J Physiol Regul Integr Comp Physiol 2011;300:R1079–R1090.

Eranki A, Cortes N, Ferencek ZG, Sikdar S. A novel application of musculoskeletal ultrasound imaging. J Vis Exp 2013;79:e50595.

Gijsbertse K, Sprengers AM, Nillesen MM, Hansen HH, Lopata RG, Verdonschot N, de Korte CL. Three-dimensional ultrasound strain imaging of skeletal muscles. Phys Med Biol 2017;62:596–611.

Hansen HH, Lopata RG, Idzenga T, de Korte CL. Full 2 D displacement vector and strain tensor estimation for superficial tissue using beam-steered ultrasound imaging. Phys Med Biol 2010;55:3201–3218.

Harding PJ, Loram ID, Combes N, Hodson-Tole EF. Ultrasound-based detection of fasciculations in healthy and diseased muscles. IEEE Trans Biomed Eng 2016;63:512–518.

Heckmatt JZ, Dubowitz V, Leeman S. Detection of pathological change in dystrophic muscle with B-scan ultrasound imaging. Lancet 1980;28:1389–1390.

Janssen BH, Pillen S, Voet NB, Heerschap A, van Engelen BG, van Alfen N. Quantitative muscle ultrasound versus quantitative magnetic resonance imaging in facioscapulohumeral dystrophy. Muscle Nerve 2014a;50:968–975.

Janssen BH, Voet NB, Nabuurs CI, Kan HE, de Rooy JW, Geurts AC, Padberg GW, van Engelen BG, Heerschap A. Distinct disease phases in muscles of facioscapulohumeral dystrophy patients identified by MR detected fat infiltration. PLoS One 2014b;9:e85416.

Lacourpaille L, Hug F, Guevel A, Pereon Y, Magot A, Hogrel JY, Nordez A. New insights on contraction efficiency in patients with Duchenne muscular dystrophy. J Appl Physiol (1985) 2014;117:658–662.

Lamperti C, Fabbri G, Vercelli L, D'Amico R, Frusciante R, Bonifazi E, Fiorillo C, Borsato C, Cao M, Servida M, Greco F, Di Leo R, Volpi L, Manzoli C, Cudia P, Pastorello E, Ricciardi L, Siciliano G, Galluzzi G, Rodolico C, Santoro L, Tomelleri G, Angelini C, Ricci E, Palmucci L, Moggio M, Tupler R. A standardized clinical evaluation of patients affected by facioscapulohumeral muscular dystrophy: The FSHD clinical score. Muscle Nerve 2010;42:213–217.

Lassche S, Stienen GJ, Irving TC, van der Maarel SM, Voermans NC, Padberg GW, Granzier H, van Engelen BG, Ottenheijm CA. Sarcomeric dysfunction contributes to muscle weakness in facioscapulohumeral muscular dystrophy. Neurology 2013;80:733–737.

Lopata RG, Nillesen MM, Hansen HH, Gerrits IH, Thijssen JM, de Korte CL. Performance evaluation of methods for two-dimensional displacement and strain estimation using ultrasound radio frequency data. Ultrasound Med Biol 2009;35:796–812.

Lopata RG, van Dijk JP, Pillen S, Nillesen MM, Maas H, Thijssen JM, Stegeman DF, de Korte CL. Dynamic imaging of skeletal muscle contraction in three orthogonal directions. J Appl Physiol (1985) 2010;109:906–915.

Lunt PW, Jardine PE, Koch MC, Maynard J, Osborn M, Williams M, Harper PS, Upadhyaya M. Correlation between fragment size at D4 F104 S1 and age at onset or at wheelchair use, with a possible generational effect, accounts for much phenotypic variation in 4q35-facioscapulohumeral muscular dystrophy (FSHD). Hum Mol Genet 1995;4:951–958.

Mazzoli V, Oudeman J, Nicolay K, Maas M, Verdonschot N, Sprengers AM, Nederveen AJ, Froeling M, Strijkers GJ. Assessment of passive muscle elongation using Diffusion Tensor MRI: Correlation between fiber length and diffusion coefficients. NMR Biomed 2016;29:1813–1824.

Moerman KM, Sprengers AM, Simms CK, Lamerichs RM, Stoker J, Nederveen AJ. Validation of continuously tagged MRI for the measurement of dynamic 3 D skeletal muscle tissue deformation. Med Phys 2012;39:1793–1810.

Mul K, van den Boogaard ML, van der Maarel SM, van Engelen BG. Integrating clinical and genetic observations in facioscapulohumeral muscular dystrophy. Curr Opin Neurol 2016;29:606–613.

Nijboer-Oosterveld J, Van Alfen N, Pillen S. New normal values for quantitative muscle ultrasound: Obesity increases muscle echo intensity. Muscle Nerve 2011;43:142–143.

Pappas GP, Asakawa DS, Delp SL, Zajac FE, Drace JE. Nonuniform shortening in the biceps brachii during elbow flexion. J Appl Physiol (1985) 2002;92:2381–2389.

Pillen S, Arts IM, Zwarts MJ. Muscle ultrasound in neuromuscular disorders. Muscle Nerve 2008;37:679–693.

Pillen S, Scholten RR, Zwarts MJ, Verrips A. Quantitative skeletal muscle ultrasonography in children with suspected neuromuscular disease. Muscle Nerve 2003;27:699–705.

Pillen S, Tak RO, Zwarts MJ, Lammens MM, Verrijp KN, Arts IM, van der Laak JA, Hoogerbrugge PM, van Engelen BG, Verrips A. Skeletal muscle ultrasound: Correlation between fibrous tissue and echo intensity. Ultrasound Med Biol 2009;35:443–446.

Pillen S, van Alfen N. Skeletal muscle ultrasound. Neurol Res 2011;33:1016–1024.

Pillen S, Verrips A, van Alfen N, Arts IM, Sie LT, Zwarts MJ. Quantitative skeletal muscle ultrasound: Diagnostic value in childhood neuromuscular disease. Neuromuscul Disord 2007;17:509–516.

Raiteri BJ, Cresswell AG, Lichtwark GA. Three-dimensional geometrical changes of the human tibialis anterior muscle and its central aponeurosis measured with three-dimensional ultrasound during isometric contractions. PeerJ 2016;4:e2260.

Reimers K, Reimers CD, Wagner S, Paetzke I, Pongratz DE. Skeletal muscle sonography: A correlative study of echogenicity and morphology. J Ultrasound Med 1993;12:73–77.

Ricci E, Galluzzi G, Deidda G, Cacurri S, Colantoni L, Merico B, Piazzo N, Servidei S, Vigneti E, Pasceri V, Silvestri G, Mirabella M, Mangiola F, Tonali P, Felicetti L. Progress in the molecular diagnosis of facioscapulohumeral muscular dystrophy and correlation between the number of KpnI repeats at the 4q35 locus and clinical phenotype. Ann Neurol 1999;45:751–757.

Scholten RR, Pillen S, Verrips A, Zwarts MJ. Quantitative ultrasonography of skeletal muscles in children: Normal values. Muscle Nerve 2003;27:693–698.

Simon NG, Noto YI, Zaidman CM. Skeletal muscle imaging in neuromuscular disease. J Clin Neurosci 2016;33:1–10.

Tasca G, Pescatori M, Monforte M, Mirabella M, Iannaccone E, Frusciante R, Cubeddu T, Laschena F, Ottaviani P, Ricci E. Different molecular signatures in magnetic resonance imaging-staged facioscapulohumeral muscular dystrophy muscles. PLoS One 2012;7:e38779.

Tawil R. Facioscapulohumeral muscular dystrophy. Neurotherapeutics 2008;5:601–606.

van Overveld PG, Enthoven L, Ricci E, Rossi M, Felicetti L, Jeanpierre M, Winokur ST, Frants RR, Padberg GW, van der Maarel SM. Variable hypomethylation of D4 Z4 in facioscapulohumeral muscular dystrophy. Ann Neurol 2005;58:569–576.

Vanhoutte EK, Faber CG, van Nes SI, Jacobs BC, van Doorn PA, van Koningsveld R, Cornblath DR, van der Kooi AJ, Cats EA, van den Berg LH, Notermans NC, van der Pol WL, Hermans MC, van der Beek NA, Gorson KC, Eurelings M, Engelsman J, Boot H, Meijer RJ, Lauria G, Tennant A, Merkies IS, PeriNom SSG. Modifying the medical research council grading system through Rasch analyses. Brain 2012;135:1639–1649.

Zaidman CM, van Alfen N. Ultrasound in the assessment of myopathic disorders. J Clin Neurophysiol 2016;33:103–111.

Zhong X, Epstein FH, Spottiswoode BS, Helm PA, Blemker SS. Imaging two-dimensional displacements and strains in skeletal muscle during joint motion by cine DENSE MR. J Biomech 2008;41:532–540.